npj | computational materials

Article

Published in partnership with the Shanghai Institute of Ceramics of the Chinese Academy of Sciences

https://doi.org/10.1038/s41524-025-01828-7

Autonomous closed-loop exploration of composition-spread films for the anomalous Hall effect

Ryo Toyama [1] ✉, Ryo Tamura [2,3] ✉, Shoichi Matsuda [4], Yuma Iwasaki [2] & Yuya Sakuraba [1] ✉

Autonomous high-throughput combinatorial experimentation is a key approach for accelerating materials discovery. However, achieving a fully closed-loop system remains a challenge due to the lack of effective optimization strategies for combinatorial experimentation. Here, we developed a Bayesian optimization method specifically designed for composition-spread films, enabling the selection of promising composition-spread films and identifying which elements should be compositionally graded. Using this approach, we demonstrated an autonomous closed-loop exploration of composition-spread films to enhance the anomalous Hall effect (AHE). Our method optimized the composition of a five-element alloy system consisting of three 3*d* ferromagnetic elements of Fe, Co, and Ni and two 5*d* heavy elements from Ta, W, or Ir to maximize the AHE. Through our autonomous exploration, we achieved a maximum anomalous Hall resistivity of 10.9 μΩ cm in $Fe_{44.9}Co_{27.9}Ni_{12.1}Ta_{3.3}Ir_{11.7}$ amorphous thin film on thermally oxidized Si substrates deposited at room temperature.

Autonomous exploration for novel materials, combining machine learning and experiments, has attracted much attention for accelerating materials discovery[1–12]. This approach aims to identify new materials with desired properties through a closed-loop system that integrates experiments, including materials synthesis and physical property measurement, with machine-learning-based selection of the next experimental conditions. Through multiple iterations of this closed-loop process, materials that exhibit the desired properties can be obtained. Around the world, self-driving laboratories equipped with robots are being developed to conduct this closed-loop exploration without human intervention[13–19].

When we focus on thin-film materials, combinatorial thin-film deposition techniques, which allow the fabrication of a large number of compounds with varying compositions on a single substrate in a single experiment, have been remarkably developed[20–34]. If this system can be integrated into an autonomous closed-loop exploration system, a significant amount of material data can be obtained in a single cycle, which is expected to further accelerate the materials discovery. However, the implementation of the combinatorial thin-film deposition technique into a closed-loop system combined with machine learning has not yet been demonstrated. The main reason for this is the lack of machine learning techniques tailored to combinatorial thin-film deposition. The algorithm must be capable of selecting the elements to be compositionally graded and predicting the multiple compositions of those elements that will exhibit the desired properties. However, conventional Bayesian optimization packages such as GPyOpt[35] and Optuna[36] cannot simply be used, as they do not allow for the selection of elements to be compositionally graded for combinatorial thin-film deposition. Therefore, a Bayesian optimization strategy tailored for combinatorial experiments is essential for closed-loop high-throughput systems.

In this study, we developed a Bayesian optimization method specifically designed for composition-spread films, enabling the selection of promising composition-spread films and identifying which elements should be compositionally graded. Using the developed method, we demonstrated autonomous closed-loop materials exploration for enhancing the anomalous Hall effect (AHE) using high-throughput combinatorial experiments and Bayesian optimization (see Fig. 1). We used combinatorial fabrication and measurement systems reported in ref. 37. The AHE is the phenomena that produces transverse spontaneous Hall voltage perpendicular to the applied electrical current and spontaneous magnetization in magnetic materials[38], which is useful for the development of various sensing devices[39,40]. Our high-throughput method consists of the deposition of composition-spread films using combinatorial sputtering (Fig. 1(i)),

[1]Research Center for Magnetic and Spintronic Materials (CMSM), National Institute for Materials Science (NIMS), Ibaraki, Japan. [2]Center for Basic Research on Materials (CBRM), National Institute for Materials Science (NIMS), Ibaraki, Japan. [3]Graduate School of Frontier Sciences, The University of Tokyo, Chiba, Japan. [4]Research Center for Energy and Environmental Materials (GREEN), National Institute for Materials Science (NIMS), Ibaraki, Japan.
✉e-mail: TOYAMA.Ryo@nims.go.jp; TAMURA.Ryo@nims.go.jp; SAKURABA.Yuya@nims.go.jp

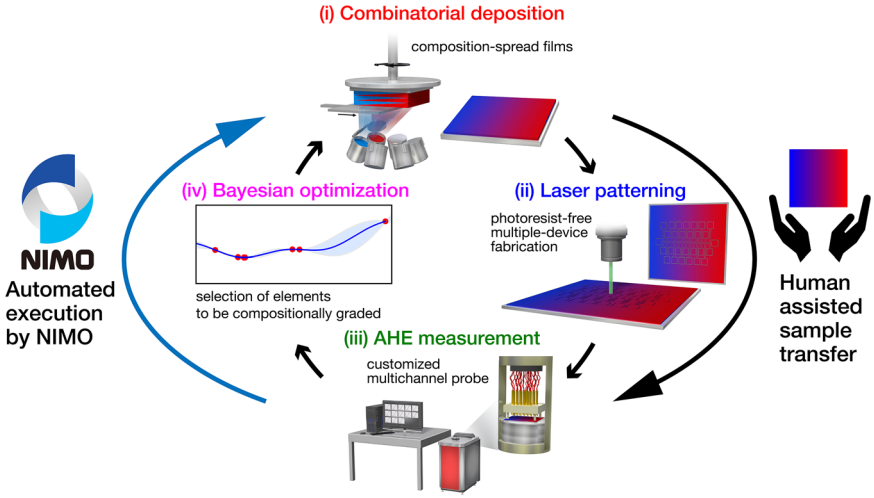

Fig. 1 | Autonomous closed-loop high-throughput materials exploration for the anomalous Hall effect (AHE) using combinatorial experiments and Bayesian optimization. This system consists of (i) deposition of composition-spread films using a combinatorial sputtering system, (ii) photoresist-free facile 13-device fabrication using a laser patterning system, (iii) simultaneous AHE measurement of 13 devices using a customized multichannel probe, and (iv) Bayesian optimization specifically designed for the composition-spread films, enabling the selection of promising composition-spread film and identifying which elements should be compositionally graded.

photoresist-free facile 13-device fabrication using laser patterning (Fig. 1(ii)), and simultaneous AHE measurement of 13 devices using a customized multichannel probe (Fig. 1(iii))[37].

In our closed-loop system, to minimize human intervention, we developed a Python program that automatically generates an input recipe file for the combinatorial sputtering system, as well as a program that automatically analyzes the results of AHE measurements and calculates anomalous Hall resistivity (ρ^A_{yx}). These programs, along with the Bayesian optimization method for composition-spread films, are implemented in NIMO (NIMS orchestration system)[41], which is the orchestration software to support autonomous closed-loop exploration and made publicly available on GitHub[42]. By executing a series of programs controlled by NIMO, we successfully developed a fully automated system that predicts the next experimental conditions from raw AHE measurement data and generates the input file for the deposition system. The only points of human intervention in the closed-loop exploration are the transfer of samples from the combinatorial sputtering system to the laser patterning system (from (i) to (ii) in Fig. 1) and from the laser patterning system to the AHE measurement system (from (ii) to (iii) in Fig. 1). Thus, apart from these sample transfers, the entire process was carried out using a fully autonomous, automated closed-loop system. Using the system, we optimized the composition of the heavy-metal-added five-element alloy system, selecting from Fe, Co, Ni, Ta, W, or Ir to maximize the ρ^A_{yx}. We also performed an analysis using a random forest model on the obtained experimental data to reveal the contribution to the enhancement of AHE.

Results

Bayesian optimization specifically designed for composition-spread films

We developed a Bayesian optimization method for composition-spread films. To implement this, we utilized a Python library PHYSBO (optimization tools for PHYSics based on Bayesian Optimization)[43]. In this study, we considered the case where a composition gradient is applied to two elements. The selection process for subsequent candidate compositions is as follows:

1. Select the composition with the highest acquisition function value using the PHYSBO package. The acquisition function is determined based on prediction results from Gaussian process regression.
2. Specify two elements to be subjected to a composition gradient. When the composition-spread film is fabricated, L types of compositions with different mixing ratios of the two elements, evenly spaced, are prepared. For these L compositions, the acquisition function values are evaluated using the PHYSBO package. Note that the compositions of the remaining elements other than the selected two elements are fixed at the values selected in Step 1.
3. Define a score for the composition-spread film when the two elements are compositionally graded by averaging the L acquisition function values.
4. Repeat Steps 2 and 3 for all possible pairs of elements that can be compositionally graded.
5. Propose the two elements to be compositionally graded that achieve the highest score. Simultaneously, suggest the L compositions with different mixing ratios of these two elements.

Step 1 is exactly the same as the conventional Bayesian optimization strategy used in, for example, ref. 3. Steps 2–5 are required in the Bayesian optimization process for composition-spread films to select the elements to be compositionally graded.

The above proposal can be executed using the newly implemented "nimo.selection" function in "COMBI" mode. If this function of NIMO is executed, the proposals are output to "proposals.csv" from "candidates.csv," where the composition candidates are stored (see Fig. 2). It is important to note that in the "COMBI" mode, the proposed compositions listed in the "proposals.csv" do not necessarily match those in the "candidates.csv." This discrepancy arises due to the nature of the combinatorial experiments, where proposed compositions will be prepared with different mixing ratios at equal intervals. Therefore, special care should be taken when updating the "candidates.csv" after obtaining the objective function values when the experiments are finished. In this study, we removed candidate compositions that fell within the composition range in the "proposals.csv" from the "candidates.csv," and we added the actual compositions and objective function values obtained from the experiments to the "candidates.csv." This operation is automatically performed using "COMBAT (cluster-type COMBinatorial sputtering system for the Anomalous hall effecT)" mode for "nimo.analysis_output" function in the NIMO package (see Fig. 2). In addition, using "nimo.preparation_input" function, an input recipe file for the combinatorial sputtering deposition system can be created from "proposals.csv" (see Fig. 2). More details for programs are provided in the "Methods" section.

Optimization of five-element alloy composition-spread films

To validate our high-throughput system using combinatorial experiments and Bayesian optimization specifically designed for composition-spread films developed in this study, we set a five-element alloy system as a search space and optimize the composition to maximize the AHE. The five-element alloy system consists of three room-temperature 3*d* ferromagnetic elements of Fe, Co, and Ni, and two 5*d* heavy elements from Ta, W, or Ir. We chose these 5*d* heavy metals as adding elements because these were the elements that tended to yield larger AHE in the previous study[37]. To prepare the candidate compositions in "candidates.csv," we set Fe, Co, and Ni to be

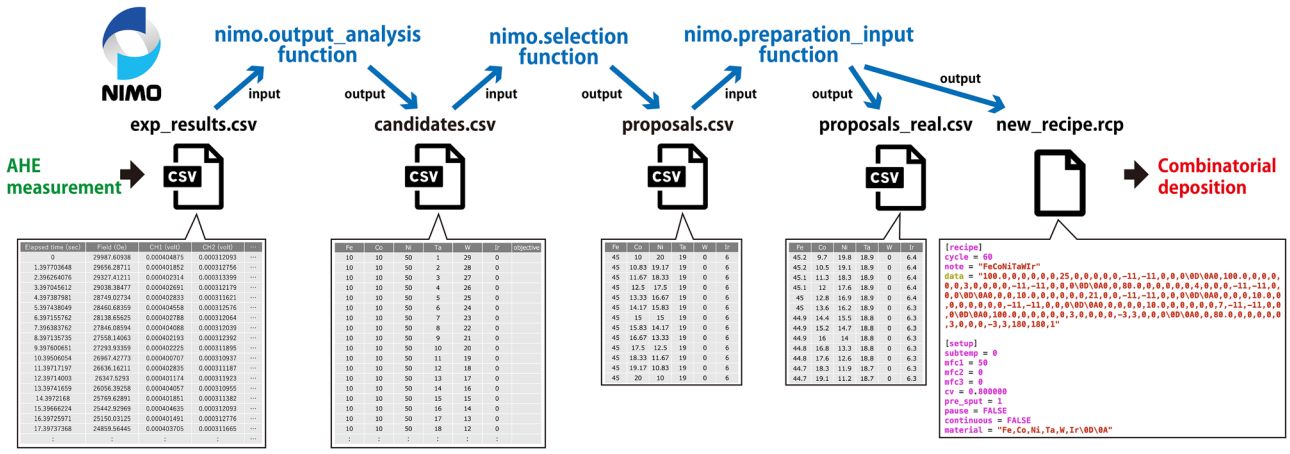

Fig. 2 | Input and output files for NIMO functions. Using three functions of "nimo.output_analysis," "nimo.selection," and "nimo.preparation_input" in NIMO, the input file for combinatorial deposition can be obtained from the raw AHE measurement results.

10–70 at.% in increments of 5 at.%, respectively, with their total amount ranging to 70–95 at.%. For the heavy metals, we set two from Ta, W, and Ir to be 1–29 at.% in increments of 1 at.%, respectively, with their total amount ranging to the remaining 30–5 at.%. This results in a total of 18594 candidates, and these candidates are stored in the "candidates.csv." The composition-spread films of the five-element alloy system were deposited, in which two of the elements are compositionally graded. One of the examples of the five-element alloy composition-spread films is shown in Fig. 3a, where the example is the case for composition gradient between Ni and Co in an Fe–Co–Ni–Ta–Ir system fabricated for the 11th cycle. The combination of elements to be compositionally graded was limited to a pair of 3*d*–3*d* or 5*d*–5*d* elements because the combination of 3*d*–5*d* elements does not produce a flat film in terms of film thickness calculation due to large differences in density and molar mass between the 3*d* and 5*d* elements. The composition-spread films were deposited on thermally oxidized Si (SiO_2/Si) substrates at room temperature. If a large AHE is obtained in the films on the amorphous surface of substrates deposited at room temperature, the films can be directly connected to practical applications. In this experiment, we aim to achieve ρ_{yx}^{A} values of over 10 μΩ cm, which is comparable to that of Fe–Sn exhibiting one of the largest ρ_{yx}^{A} values as room-temperature-deposited magnetic thin films[44,45]. The AHE measurement was performed at room temperature (300 K). One of the examples of the AHE curves of composition-spread films is also shown in Fig. 3b, which was obtained from the 11th cycle. In this study, the deposition of five-element alloy composition-spread films took ≈1–2 h, the device fabrication by laser patterning took ≈1.5 h, and the simultaneous AHE measurement took ≈0.2 h. Thus, one full closed-loop cycle was completed within ≈3–4 h. More details are provided in the "Methods" section.

In the first cycle of exploration, one composition-spread film was randomly selected by specifying "RE" for the "physbo_score" parameter in the "nimo.selection" function with the "COMBI" mode. In our combinatorial experimental system, 13 data are obtained simultaneously; therefore, "num_proposals" was set to 13. In the 1st cycle, the Ta–W-containing system was selected. To prepare the input recipe file for the sputtering system, the "nimo.preparation_input" function was used with the "COMBAT" mode. Using the generated recipe file, the deposition of composition-spread film was performed using a combinatorial sputtering system, followed by photoresist-free facile fabrication of 13 devices and simultaneous AHE measurements. From the AHE measurements, ρ_{yx}^{A} was automatically calculated using the "COMBAT" mode in the "nimo.analysis_output" function within the NIMO package. Subsequently, the next experimental conditions were selected by the "nimo.selection" function in the NIMO. To obtain training data for Bayesian optimization, for the first three cycles, we performed the AHE experiments based on randomly proposed compositions containing all of the combinations for the heavy metals ([Ta, W], [Ir, Ta], and [W, Ir]) (Fig. 3c(i)). Here, the initial conditions were generated randomly because only three initial cycles were performed. However, if more initial cycles are conducted, an active learning-based strategy for selecting initial conditions could be more effective. A relatively large ρ_{yx}^{A} of 7.9 μΩ cm was obtained in the W–Ir-containing system in the 3rd cycle. After the 4th cycle, the Bayesian optimization method specifically designed for composition-spread films was used by specifying "EI" for the "physbo_score" parameter in the "nimo.selection" function with the "COMBI" mode. The explanatory variables are the six-dimensional elemental composition. Here, the cycle dependence on ρ_{yx}^{A} values of five-element alloy composition-spread thin films is summarized in Fig. 3c.

Between the 4th and 8th cycles, the Bayesian optimization method proposed only the W–Ir-containing system (Fig. 3c(ii)). This is because a relatively large ρ_{yx}^{A} of 7.9 μΩ cm was obtained in the W–Ir system by chance in the first three cycles based on the random exploration. However, the ρ_{yx}^{A} values between the 4th and 8th cycles did not exceed 7.9 μΩ cm obtained in the 3rd cycle. Based on the experimental results for the W–Ir system from the 4th to 8th cycle, we judged that it would be difficult to find compositions in the W–Ir system that exceed the ρ_{yx}^{A} value obtained in the 3rd cycle. Then, we shifted to the problem of identifying optimal compositions in the Ta–W and Ta–Ir systems that exhibit larger ρ_{yx}^{A}. We performed the Bayesian optimization in the search space, omitting the W–Ir system from the 9th cycle. The search in NIMO was easily performed by simply removing the W–Ir entries that had not yet been tested from the candidate compositions in the "candidates.csv." After removing the search space for the W–Ir system, we performed the experiments from the 9th to 14th cycle (Fig. 3c(iii)). For all 6 cycles, the Ta–Ir system was proposed, and ρ_{yx}^{A} values beyond 7.9 μΩ cm were obtained. A maximum ρ_{yx}^{A} of 10.9 μΩ cm was obtained for $Fe_{44.9}Co_{27.9}Ni_{12.1}Ta_{3.3}Ir_{11.7}$ in the 11th cycle. After the 14th cycle, we judged that maximum ρ_{yx}^{A} would no longer be updated in the Ta–Ir system, so we removed the search space for the Ta–Ir system and finally moved on to the search for optimal composition in the remaining Ta–W system. The experiments for the Ta–W system were performed for 4 cycles from the 15th to 18th cycle (Fig. 3c(iv)). The obtained ρ_{yx}^{A} values were as low as below 3 μΩ cm, although it has improved compared to the initial random sampling results. Thus, we stopped the experiments after the 18th cycle.

As a result, out of 18 cycles that contain 234 compositions in total, a maximum ρ_{yx}^{A} of 10.9 μΩ cm was achieved for $Fe_{44.9}Co_{27.9}Ni_{12.1}Ta_{3.3}Ir_{11.7}$ in the autonomous closed-loop system with minimal human intervention, which was beyond the values obtained in the first three cycles based on the random exploration. Based on the X-ray diffraction (XRD) patterns as shown in Fig. 4, the film deposited on SiO_2/Si substrates at room temperature was an amorphous structure, as evident by no obvious diffraction

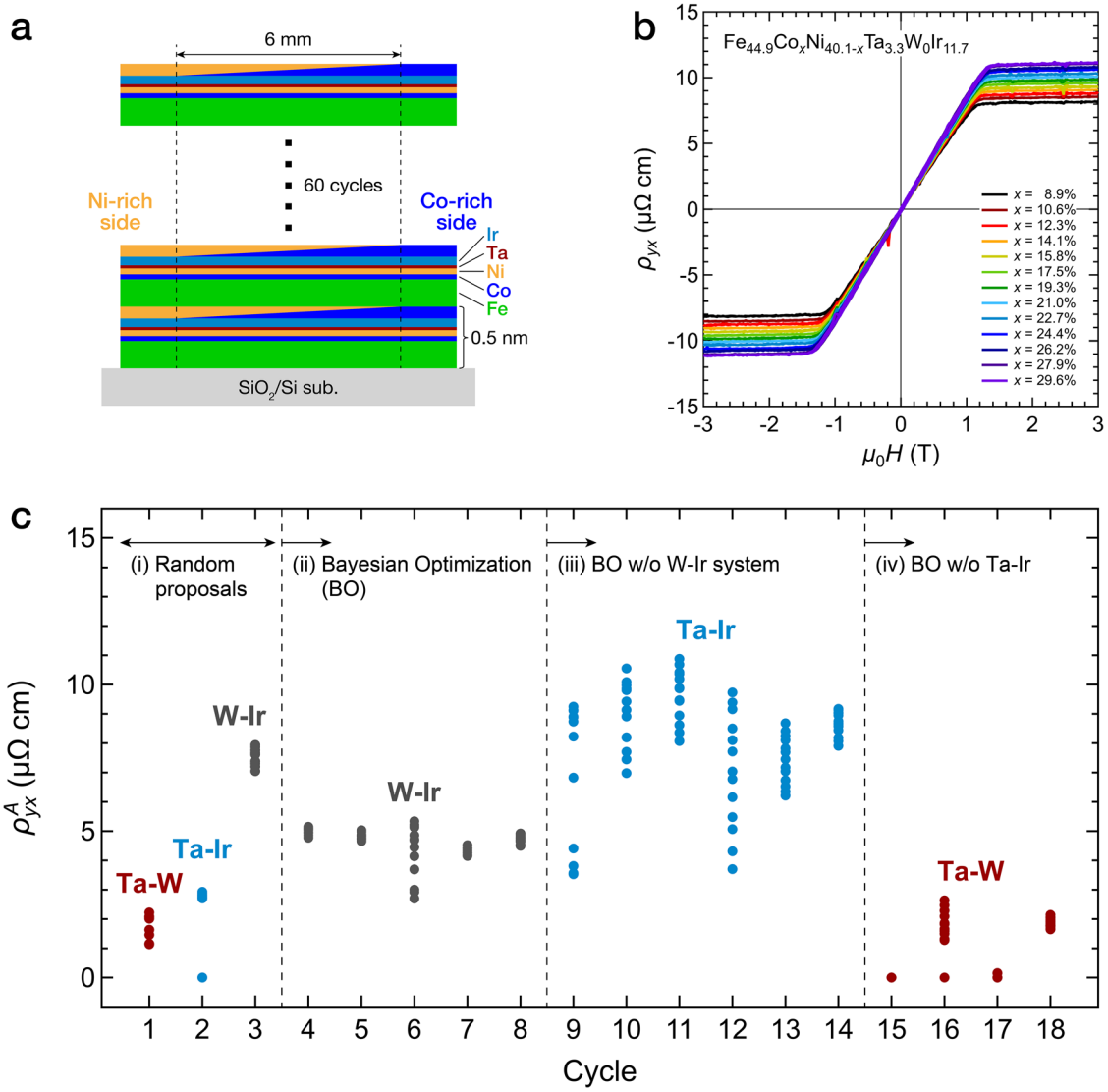

Fig. 3 | AHE in five-element alloy composition-spread films. a Schematic illustration for one of the examples of five-element alloy composition-spread films consisting of three room-temperature 3*d* ferromagnetic elements of Fe, Co, and Ni, and two 5*d* heavy elements from Ta, W, or Ir. This example is the case for composition gradient between Ni and Co in an Fe–Co–Ni–Ta–Ir composition-spread film obtained for the 11th cycle. **b** Magnetic-field (*H*)-dependent Hall resistivity (ρ_{yx}) curves for the composition-spread film shown in **a**. **c** Plots for anomalous Hall resistivity (ρ_{yx}^{A}) against closed-loop cycles.

peaks. Thus, the amorphous thin film with this optimal composition exhibiting a large ρ_{yx}^{A} of over 10 μΩ cm that can be fabricated on non-crystalline surfaces would be beneficial to practical device applications.

Discussion

To confirm the prediction performance in the Bayesian optimization, ρ_{yx}^{A} values for the five-element alloy composition-spread films were predicted based on the experimentally obtained 234 data by 10-fold cross validations using the Gaussian process regression. Here, the six-dimensional elemental composition was used as features. The coefficient of determination (R^2) between the predicted and real ρ_{yx}^{A} values was 0.9429 (Fig. S1 in the Supplementary Information), which indicates that the ρ_{yx}^{A} values can be predicted with high accuracy. Given the high prediction accuracy of the Gaussian process model, Bayesian optimization can be regarded as an efficient search strategy.

Using the Gaussian process regression, the distribution of ρ_{yx}^{A} values in the six-dimensional elemental composition space can be predicted, which is shown in Fig. S2. First, when the amount of 3*d* ferromagnetic elements is too small (70% case), the value of ρ_{yx}^{A} does not tend to increase. This would be because the ferromagnetic elements are too few for ferromagnetism to appear in the five-element alloy system at 300 K (ref. 46). In the Ta–Ir system, which exhibits the largest ρ_{yx}^{A}, an excessive amount of Ta suppresses the ρ_{yx}^{A}, while a higher Ir composition is preferable. Even when the amount of 3*d* ferromagnetic elements is too high (90% case), the ρ_{yx}^{A} value remains small. This suggests that optimizing the balance between the 3*d* ferromagnetic elements and 5*d* heavy elements is crucial, as well as selecting the appropriate 5*d* elements.

To address the importance of elements to enhance the ρ_{yx}^{A}, we also performed an analysis using a random forest model on the obtained data. The R^2 value was 0.9755 (Fig. 5a) when 10-fold cross validation was performed, which shows high accuracy for predicting the ρ_{yx}^{A} values using the composition as features. To evaluate the contribution of each element to the predicted ρ_{yx}^{A} values, we performed SHAP (SHapley Additive exPlanations) analysis[47]. Figure 5b shows a beeswarm plot, indicating SHAP values for each explanatory variable (six elements). Because the contribution to the prediction of ρ_{yx}^{A} becomes greater as the SHAP value becomes larger, the element with a wider distribution on the SHAP value (horizontal axis) is more important. From Fig. 5b, Ir has the widest distribution of the SHAP values, indicating that Ir has the greatest impact on the predicted ρ_{yx}^{A} values among the six elements. The SHAP value for Ir becomes larger for a higher

feature value. Thus, Ir composition has a positive correlation with the ρ_{yx}^{A} values; the ρ_{yx}^{A} becomes larger as the Ir composition increases. Similarly, for Fe, the ρ_{yx}^{A} values are found to be larger when more Fe is added. On the other hand, for the third most important element, Ni, the SHAP value becomes smaller as the feature value increases, which indicates a negative correlation between Ni composition and the ρ_{yx}^{A} values. In other words, the ρ_{yx}^{A} values can be larger with less Ni composition. Therefore, it is revealed that the addition of Ir and Fe increases the ρ_{yx}^{A} of the five-element alloy system. This analysis result can be understood qualitatively that Ir contributes to enhance the AHE by increasing the extrinsic and/or intrinsic contributions through stronger spin–orbit coupling[33,48], while the magnetic moment of Fe–Co–Ni alloys tends to increase with increasing Fe composition according to the Slater–Pauling curve[49–51], which leads to a larger ρ_{yx}^{A} if we simply assume a linear dependence of magnetization and the AHE[52].

To summarize, we conducted an autonomous closed-loop exploration of composition-spread films to enhance the AHE using combinatorial experiments and Bayesian optimization. To achieve this, we developed a Bayesian optimization method specifically designed for composition-spread films, enabling the selection of promising composition-spread films and identifying which elements should be compositionally graded. As a result, we discovered that an $Fe_{44.9}Co_{27.9}Ni_{12.1}Ta_{3.3}Ir_{11.7}$ amorphous thin film exhibits a large ρ_{yx}^{A} of 10.9 μΩ cm. We believe that our Bayesian optimization strategy for composition-spread films is one of the key technologies to advance autonomous closed-loop materials exploration using combinatorial experiments.

Finally, we discuss future prospects. In the current closed-loop system, automation has been implemented except for the manual transfer of samples between experimental instruments. To achieve a fully automated closed-loop system without human intervention, robotics such as sample-transfer robots should be introduced. This would enable the development of a fully automated and self-driving materials exploration platform. Once such a system is completed, continuous improvement will be essential to fit diverse materials discovery needs. Our platform enables closed-loop materials development through three core components, each of which needs further enhancement. The first is the improvement of the thin-film deposition system. In this study, we focused on a linear composition gradient for two elements. Introducing gradients of more elements would allow the simultaneous fabrication of a wider variety of materials. While our current setup supports up to three-element gradients (i.e., two-dimensional composition-spread films), accommodating four or more elements requires hardware modifications to the deposition instrument. The second is the expansion of measurement capabilities. By incorporating various automatic prober systems for thin films, we will aim to perform additional measurements such as magnetoresistance and thermoelectric measurements, thereby increasing the system's versatility. The third is the improvement of the search algorithm. The current Bayesian optimization program can only handle the composition gradient of two elements. It needs to be improved to accommodate combinatorial deposition systems that can fabricate samples with composition gradients of more than two elements. In addition, beyond compositional optimization, it is also important to optimize deposition parameters such as deposition temperature, deposition pressure, and gas flow. To support this, the Bayesian optimization program must be extended to handle a broader range of variables. These improvements will enhance the capability of our system for materials development. Thus, we will continue to refine the optimization method alongside the development of experimental equipment, thereby realizing autonomous, automated, high-throughput materials discovery through combinatorial experiments.

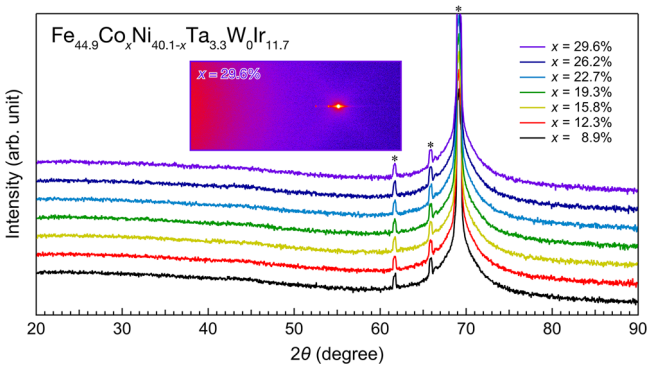

Fig. 4 | X-ray diffraction (XRD) patterns of Fe–Co–Ni–Ta–Ir composition-spread film obtained for the 11th cycle. The inset shows a two-dimensional XRD image as a typical result. The diffraction peaks from SiO_2/Si substrates are indicated by the symbol *. The film structure is shown in Fig. 3a.

Methods

High-throughput combinatorial AHE experiments

The AHE experiments were performed using a high-throughput method that combines deposition of composition-spread films using combinatorial sputtering, photoresist-free facile 13-device fabrication using laser patterning, and simultaneous AHE measurement of 13 devices using a customized multichannel probe. The details of the method are described in the previous study[37]. Briefly, composition-spread films were deposited on thermally oxidized Si (SiO_2/Si) substrates with a size of 10 mm by 10 mm at room temperature using a combinatorial magnetron sputtering system (CMS-A6250X2, Comet Inc.). The Ar process gas pressure was set to 0.8 Pa. The composition-spread film consists of three room-temperature 3*d* ferromagnetic elements of Fe, Co, and Ni, and two 5*d* heavy metals from Ta, W, or Ir, with two of the elements (*X* and *Y*) being compositionally graded (see Fig. 3a as an example with *X* = Co and *Y* = Ni). The six elemental targets were installed in the deposition chamber. The deposition rate for each target at a fixed power was determined using X-ray reflectometry (XRR) prior to the combinatorial deposition. To fabricate five-element

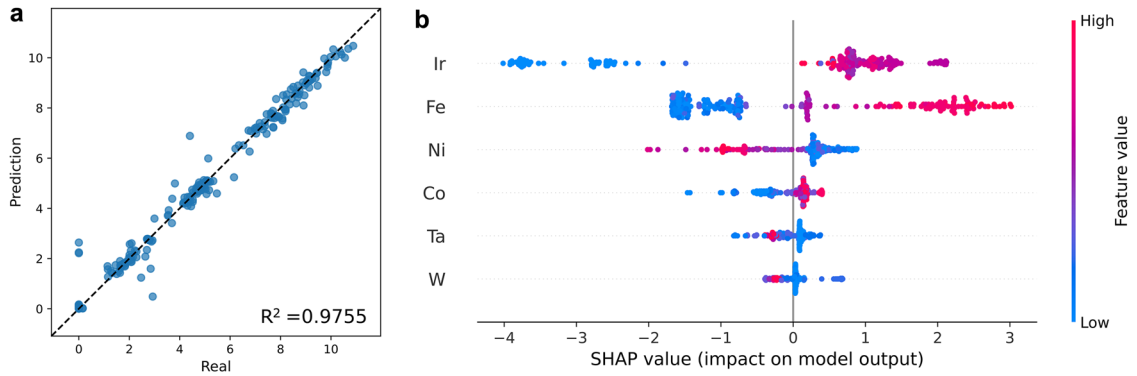

Fig. 5 | Analysis results by the random forest model. a Prediction of ρ_{yx}^{A} values when 10-fold cross validation was performed. **b** Beeswarm plot for SHAP (SHapley Additive exPlanations) values and the six elements.

alloy composition-spread films, uniform layers of five elements were first deposited on the substrate sequentially. Then, a wedge-shaped *X* layer was deposited on the uniform multilayers with a composition gradient width of 6 mm using a linear moving mask. Subsequently, the substrate was rotated by 180°, and a wedge-shaped *Y* layer was deposited on the wedge-shaped *X* layer with the same thickness and composition gradient width. The combination of elements to be compositionally graded was limited to a pair of 3*d*–3*d* or 5*d*–5*d* elements because the combination of 3*d*–5*d* elements does not produce a flat film in terms of film thickness calculation due to large differences in density and molar mass between the 3*d* and 5*d* elements. The total thickness for the one-unit layer consisting of five uniform layers and two wedge-shaped layers was set to 0.5 nm. The partial thickness of each uniform layer and wedge-shaped layer was designed so that compositions proposed by the Bayesian optimization were obtained at the *X*- and *Y*-richest regions in the composition-spread film. The deposition process for the one-unit layer was repeated 60 times to obtain 30-nm-thick films. After the deposition, the films were capped with Al (2 nm) to prevent oxidation. The composition-spread film was patterned into 13 Hall bar devices using a laser patterning system (VL-C30-RGBV, Sigmakoki Co., Ltd.). The device consists of 14 pairs of terminals, including 13 pairs perpendicular to the composition gradient for Hall voltage measurements, connected to one pair for a common electrical current path along the composition gradient. The AHE of 13 devices in the composition-spread film was measured simultaneously using a customized multichannel probe. The probe consists of a sample holder and a pin block array containing 28 spring-loaded pins (pogo-pins) to match the locations of the 28 electrical contact pads for the 14 pairs of terminals of the laser-patterned devices. After setting the sample on the sample holder, the pin block array was pressed onto the sample to make electrical contacts. After that, the probe was inserted into a chamber of the physical property measurement system (PPMS Versalab, Quantum Design). The Hall voltage was measured with a constant electrical current of 0.2 mA while the perpendicular magnetic field was swept using the PPMS. The AHE measurement was performed at room temperature (300 K).

Bayesian optimization program for composition-spread films

The developed Bayesian optimization program for composition-spread films was implemented in the "nimo.selection" function as "COMBI" mode. This implementation allows users to specify composition ranges for each element. Additionally, a list of two elements that can be selected for the composition gradient is defined. Specifically, the following commands can be used to make selections:

```
nimo.selection(method = "COMBI",
input_file = "candidates.csv",
output_file = "proposals.csv",
num_objectives = 1,
num_proposals = 13,
physbo_score = "EI",
combi_ranges = [[10,70], [10,70], [10,70], [1,29], [1,29], [1,29]],
spread_elements = [[0,1], [1,2], [2,0], [3,4], [4,5], [5,3]])
```

The composition candidates are stored in the file "candidates.csv," and the proposals are output to "proposals.csv" (see Fig. 2). In "candidates.csv," each row corresponds to a composition of elements, and if the experiments were finished, the objective function values (anomalous Hall resistivity) are denoted in the "objective" column. The composition with the highest acquisition function value in Step 1 is selected from rows where the objective function column is blank. The number of compositions with different mixing ratios of the two elements, denoted as *L*, is determined by the number of proposals specified in the "num_proposals," and in "proposals.csv," *L* compositions are proposed (see Fig. 2). The parameter "physbo_score" specifies the type of acquisition function calculated using Gaussian process regression, which can be selected from the following options:

- "EI": Expected Improvement
- "PI": Probability of Improvement
- "TS": Thompson Sampling
- "RE": Random Exploration

In the "combi_ranges," the composition ranges for each element are specified in the order corresponding to the columns in the "candidates.csv." In the "spread_elements," all possible pairs of elements are defined using integer indices that indicate their positions in the "candidates.csv." For example, in our case, six elements (Fe, Co, Ni, Ta, W, and Ir) were considered. The composition ranges for the 3*d* ferromagnetic elements were set from 10 to 70%, while those for the 5*d* heavy elements range from 1 to 29%, respectively. Additionally, the possible pairs for composition gradient were set to [Fe, Co], [Co, Ni], [Ni, Fe], [Ta, W], [W, Ir], and [Ir, Ta]. In other words, for the 3*d* and 5*d* elements, only elements within the same category could be compositionally graded. The program was implemented in such a way that the element is excluded from the composition gradient if the proposed composition of an element to be graded is 0 or if the composition gradient is impossible.

Preparation program for the input file of the combinatorial deposition system

Using the "nimo.preparation_input" function (see Fig. 2), an input recipe file for the combinatorial sputtering deposition system can be created with the following commands:

```
nimo.preparation_input(machine = "COMBAT",
input_file = "proposals.csv",
input_folder = input_folder)
```

In "proposals.csv," compositions for the next experiment are stored. Based on the composition information, the deposition recipe is generated using the values of density, molar mass, sputtering power, and deposition rate of each element. The file "new_recipe.rcp" is created in the folder specified by "input_folder," which is the recipe file for the next experiment. An example of a recipe file is shown in Fig. 2, where Ta and Ir are compositionally graded. In addition, when conducting combinatorial deposition, the compositions of the fabricated samples may slightly deviate from those in the "proposals.csv" due to experimental constraints. To address this, the "proposals_real.csv" file is implemented to record the actual compositions of the fabricated samples (see Fig. 2).

Automatic analysis program for AHE curves

We developed a Python program to obtain ρ_{yx}^{A} values from Hall voltage (V_{yx})–magnetic field (H) curves. The Hall resistivity (ρ_{yx}) was calculated using $\rho_{yx} = V_{yx} \cdot t/I$, where t is the film thickness and I is the applied electric current. The t and I in this study were 30 nm and 0.2 mA, respectively. The anomalous term of ρ_{yx}, that is ρ_{yx}^{A}, was obtained using $\rho_{yx}^{A} = \left(\rho_{yx}^{+} - \rho_{yx}^{-}\right)/2$, where $\rho_{yx}^{+(-)}$ represents the value obtained by extrapolating the H-dependent ρ_{yx} curves in the saturation region from positive (negative) to zero field with a linear function. For extrapolation, the data for $H > 2.5$ kOe was used to calculate ρ_{yx}^{+}, while the data for $H < -2.5$ kOe was used for ρ_{yx}^{-}. If a significant deviation was confirmed when extrapolating with a linear function or if $\rho_{yx}^{A} < 0$, ρ_{yx}^{A} was set to 0. Additionally, if the measured data was unstable, such as with many outliers, ρ_{yx}^{A} was not calculated, and a blank was returned in the "candidates.csv"; the data was not used for training data.

The calculation of ρ_{yx}^{A} values can be performed in NIMO's "COMBAT" mode using the following commands:

```
nimo.analysis_output(machine = "COMBAT",
input_file = "proposals_real.csv",
output_file = "candidates.csv",
num_objectives = 1,
output_folder = output_folder)
```

The file "exp_results.csv" is prepared in the folder specified by "output_folder." The "exp_results.csv" file stores magnetic field values in the second column and the Hall voltage obtained from the experiments in the subsequent columns (see Fig. 2). Each column corresponds to data for one

composition. Based on these results, ρ_{yx}^{A} is automatically calculated, and "candidates.csv" is updated. Additionally, the composition information is updated simultaneously by entering the actual experimental composition values into "proposals_real.csv."

X-ray diffraction (XRD)

The two-dimensional (2D) XRD images of the composition-spread films were measured using a high-resolution XRD system (SmartLab, Rigaku). The X-ray with Cu-$K\alpha$ radiation was collimated using a 0.5 mm incident slit. The one-dimensional (1D) XRD patterns were obtained from the 2D XRD images using instrument software (2DP, SmartLab Studio II; Rigaku).

Data availability

All data supporting the findings of this study are available from the corresponding authors upon reasonable request.

Code availability

All programs to generate the data of this study are available from the NIMO package (https://github.com/NIMS-DA/nimo).

Received: 15 March 2025; Accepted: 10 October 2025;
Published online: 19 November 2025

References

1. Lookman, T. et al. Active learning in materials science with emphasis on adaptive sampling using uncertainties for targeted design. *npj Comput. Mater.* **5**, 21 (2019).
2. Wakabayashi, Y. K. et al. Machine-learning-assisted thin-film growth: Bayesian optimization in molecular beam epitaxy of $SrRuO_3$ thin films. *APL Mater.* **7**, 101114 (2019).
3. Ohkubo, I. et al. Realization of closed-loop optimization of epitaxial titanium nitride thin-film growth via machine learning. *Mater. Today Phys.* **16**, 100296 (2021).
4. Tamura, R. et al. Machine learning-driven optimization in powder manufacturing of Ni-Co based superalloy. *Mater. Des.* **198**, 109290 (2021).
5. Ni, Z. & Matsui, H. Phase control of heterogeneous $Hf_xZr_{(1-x)}O_2$ thin films by machine learning. *Jpn. J. Appl. Phys.* **61**, SH1009 (2022).
6. Biswas, A. et al. A dynamic Bayesian optimized active recommender system for curiosity-driven partially Human-in-the-loop automated experiments. *npj Comput. Mater.* **10**, 29 (2024).
7. Ishiyama, T. et al. Bayesian optimization-driven enhancement of the thermoelectric properties of polycrystalline III-V semiconductor thin films. *NPG Asia Mater.* **16**, 17 (2024).
8. Harris, S. B. et al. Autonomous synthesis of thin film materials with pulsed laser deposition enabled by in situ spectroscopy and automation. *Small Methods* **8**, 2301763 (2024).
9. Shrivastava, A. et al. Bayesian optimization for stable properties amid processing fluctuations in sputter deposition. *J. Vac. Sci. Technol. A.* **42**, 033408 (2024).
10. Tamura, R. et al. AIPHAD, an active learning web application for visual understanding of phase diagrams. *Commun. Mater.* **5**, 139 (2024).
11. Cakan, D. N. et al. Bayesian optimization and prediction of the durability of triple-halide perovskite thin films under light and heat stressors. *Mater. Adv.* **6**, 598 (2025).
12. You, W. et al. Machine learning strategy for optimizing multiple electrical characteristics in dual-layer oxide thin film transistors. *ACS Appl. Mater. Interfaces* **17**, 1565–1575 (2025).
13. Burger, B. et al. A mobile robotic chemist. *Nature* **583**, 237–249 (2020).
14. Shimizu, R. et al. Autonomous materials synthesis by machine learning and robotics. *APL Mater.* **8**, 111110 (2020).
15. Matsuda, S., Lambard, G. & Sodeyama, K. Data-driven automated robotic experiments accelerate discovery of multi-component electrolyte for rechargeable Li–O_2 batteries. *Cell Rep. Phys. Sci.* **3**, 100832 (2022).
16. Szymanski, N. J. et al. An autonomous laboratory for the accelerated synthesis of novel materials. *Nature* **624**, 86–97 (2023).
17. Low, A. K. Y. et al. Evolution-guided Bayesian optimization for constrained multi-objective optimization in self-driving labs. *npj Comput. Mater.* **10**, 104 (2024).
18. Tom, G. et al. Self-driving laboratories for chemistry and materials science. *Chem. Rev.* **124**, 9633–9732 (2024).
19. Yoshikawa, N. et al. Self-driving laboratories in Japan. *Digit. Discov.* **4**, 1384–1403 (2025).
20. Ludwig, A. et al. Development of multifunctional thin films using high-throughput experimentation methods. *Int. J. Mater. Res.* **99**, 1144–1149 (2008).
21. Jin, K. et al. Combinatorial search of superconductivity in Fe-B composition spreads. *APL Mater.* **1**, 042101 (2013).
22. Kusne, A. G. et al. On-the-fly machine-learning for high-throughput experiments: search for rare-earth-free permanent magnets. *Sci. Rep.* **4**, 6367 (2014).
23. Ludwig, A. Discovery of new materials using combinatorial synthesis and high-throughput characterization of thin-film materials libraries combined with computational methods. *npj Comput. Mater.* **5**, 70 (2019).
24. Kusne, A. G. et al. On-the-fly closed-loop materials discovery via Bayesian active learning. *Nat. Commun.* **11**, 5966 (2020).
25. Masuda, H. et al. Large spin-Hall effect in non-equilibrium binary copper alloys beyond the solubility limit. *Commun. Mater.* **1**, 75 (2020).
26. Iwasaki, Y. et al. Machine learning autonomous identification of magnetic alloys beyond the Slater-Pauling limit. *Commun. Mater.* **2**, 31 (2021).
27. Modak, R. et al. Combinatorial tuning of electronic structure and thermoelectric properties in $Co_2MnAl_{1-x}Si_x$ Weyl semimetals. *APL Mater.* **9**, 031105 (2021).
28. Hong, Y. et al. A high throughput study of both compositionally graded and homogeneous Fe–Pt thin films. *J. Mater. Res. Technol.* **18**, 1245–1255 (2022).
29. Padhy, S. P. et al. Rapid multi-property assessment of compositionally modulated Fe-Co-Ni thin film material libraries. *Results Mater.* **14**, 100283 (2022).
30. Modak, R. et al. Sm-Co-based amorphous alloy films for zero-field operation of transverse thermoelectric generation. *Sci. Technol. Adv. Mater.* **23**, 767–782 (2022).
31. Suzuki, S. et al. Accelerating the combinatorial optimization process for phosphor materials by Bayesian optimization. *Jpn. J. Appl. Phys.* **62**, 117001 (2023).
32. Toyama, R. et al. Combinatorial optimization for high spin polarization in Heusler alloy composition-spread thin films by anisotropic magnetoresistance effect. *APL Mater.* **11**, 101127 (2023).
33. Toyama, R., Zhou, W. & Sakuraba, Y. Extrinsic contribution to the anomalous Hall effect and Nernst effect in Fe_3Co single-crystal thin films by Ir doping. *Phys. Rev. B* **109**, 054415 (2024).
34. Toyama, R. et al. Large anomalous Nernst conductivity of $L1_0$-ordered CoPt in CoPt composition-spread thin films. *J. Phys. D Appl. Phys.* **57**, 405001 (2024).
35. GPyOpt package. http://github.com/SheffieldML/GpyOpt
36. Optune package. https://optuna.org/
37. Toyama, R. et al. High-throughput materials exploration system for the anomalous Hall effect using combinatorial experiments and machine learning. *npj Comput. Mater.* **11**, 269 (2025).
38. Nagaosa, N. et al. Anomalous Hall effect. *Rev. Mod. Phys.* **82**, 1539–1592 (2010).
39. Shiogai, J. et al. Three-dimensional sensing of the magnetic-field vector by a compact planar-type Hall device. *Commun. Mater.* **2**, 102 (2021).
40. Nakatani, T. et al. Perspective on nanoscale magnetic sensors using giant anomalous Hall effect in topological magnetic materials for read head application in magnetic recording. *Appl. Phys. Lett.* **124**, 070501 (2024).

41. Tamura, R., Tsuda, K. & Matsuda, S. NIMS-OS: an automation software to implement a closed loop between artificial intelligence and robotic experiments in materials science. *Sci. Technol. Adv. Mater. Methods* **3**, 2232297 (2023).
42. NIMO package. https://github.com/NIMS-DA/nimo.
43. Motoyama, Y. et al. Bayesian optimization package: PHYSBO. *Comput. Phys. Commun.* **278**, 108405 (2022).
44. Satake, Y. et al. Fe-Sn nanocrystalline films for flexible magnetic sensors with high thermal stability. *Sci. Rep.* **9**, 3282 (2019).
45. Fujiwara, K. et al. Berry curvature contributions of kagome-lattice fragments in amorphous Fe–Sn thin films. *Nat. Commun.* **14**, 3399 (2023).
46. Karel, J. et al. Unexpected dependence of the anomalous Hall angle on the Hall conductivity in amorphous transition metal thin films. *Phys. Rev. Mater.* **4**, 114405 (2020).
47. Lundberg, S. M. & Lee, S.-I. A unified approach to interpreting model predictions. In *Proc. 31st International Conference on Neural Information Processing Systems* 4768–4777 https://dl.acm.org/doi/proceedings/10.5555/3295222 (Curran Associates Inc., 2017).
48. Jamaluddin, S. et al. Extrinsic to intrinsic mechanism crossover of anomalous Hall effect in the Ir-doped MnPtSn Heusler system. *Phys. Rev. B* **106**, 184424 (2022).
49. Jartych, E. On the magnetic properties of mechanosynthesized Co–Fe–Ni ternary alloys. *J. Magn. Magn. Mater.* **323**, 209–216 (2011).
50. Shamsutdinov, G. et al. Magnetization–structure– composition phase diagram mapping in Co-Fe-Ni alloys using diffusion multiples and scanning Hall probe microscopy. *Sci. Rep.* **12**, 1957 (2022).
51. Wang, J. et al. An in-situ high-throughput study of the Invar effect in the Fe–Ni–Co system. *J. Alloy. Compd.* **1010**, 177755 (2025).
52. Zeng, C. et al. Linear magnetization dependence of the intrinsic anomalous Hall effect. *Phys. Rev. Lett.* **96**, 037204 (2006).

Acknowledgements

The authors thank P. D. Kulkarni, H. Suto, and T. Nakatani from NIMS for the development of the customized multichannel probe and measurement system for the AHE. The authors thank T. Hiroto from NIMS for the technical support with the XRD measurement. This work was supported by JST CREST (Grant No. JPMJCR21O1), JST ERATO "Magnetic Thermal Management Materials Project" (Grant No. JPMJER2201), JST PRESTO (Grant No. JPMJPR24T8), MEXT Program: Data Creation and Utilization-Type Material Research and Development Project (Digital Transformation Initiative Center for Magnetic Materials; Grant No. JPMXP1122715503, and Digital Transformation Initiative for Green Energy Materials; Grant No. JPMXP1121467561), and JSPS KAKENHI Grants-in-Aid for Scientific Research (B) (Grant No. JP21H01608).

Author contributions

All the authors conceived the original idea and designed the experiment. R.Toyama carried out the experiment. R.Tamura developed the Bayesian optimization method specifically designed for composition-spread films and performed the analysis. R.Toyama and R.Tamura wrote the original manuscript. All the authors discussed the results, commented on the manuscript, and approved the final version of the manuscript.

Competing interests

The authors declare no competing interests.

Additional information

Supplementary information The online version contains supplementary material available at https://doi.org/10.1038/s41524-025-01828-7.

Correspondence and requests for materials should be addressed to Ryo Toyama, Ryo Tamura or Yuya Sakuraba.